Imaging biofilm in porous media using X-ray computed microtomography

Yohan Davit, Gabriel Iltis, Gerald Debenest, Stéphanie Veran-Tissoires, Dorthe Wildenschild, Magali Gerino, Michel Quintard

Imaging biofilm in porous media using X-ray computed microtomography

Y. DAVIT*‡,G. ILTIS||, G. DEBENEST*,†,
S. VERAN-TISSOIRES*, D. WILDENSCHILD||, M. GERINO‡,§
& M. QUINTARD*,†

*Université de Toulouse; INPT, UPS; IMFT(Institut de Mécanique des Fluides de Toulouse), Allée Camille Soula Toulouse, France

†CNRS; IMFT F-31400 Toulouse, France

‡Université de Toulouse; INPT, UPS; ECOLAB Rue Jeanne Marvig F-31055 Toulouse, France

§CNRS; ECOLAB F-31055 Toulouse, France

||School of Chemical, Biological, and Environmental Engineering, Oregon State University Corvallis, Oregon, U.S.A.

Key words: Biofilm, imaging, porous media, X-ray tomography.

Summary

In this study, a new technique for three-dimensional imaging of biofilm within porous media using X-ray computed microtomography is presented. Due to the similarity in X-ray absorption coefficients for the porous media (plastic), biofilm and aqueous phase, an X-ray contrast agent is required to image biofilm within the experimental matrix using X-ray computed tomography. The presented technique utilizes a medical suspension of barium sulphate to differentiate between the aqueous phase and the biofilm. Potassium iodide is added to the suspension to aid in delineation between the biofilm and the experimental porous medium. The iodide readily diffuses into the biofilm while the barium sulphate suspension remains in the aqueous phase. This allows for effective differentiation of the three phases within the experimental systems utilized in this study. The behaviour of the two contrast agents, in particular of the barium sulphate, is addressed by comparing two-dimensional images of biofilm within a pore network obtained by (1) optical visualization and (2) X-ray absorption radiography. We show that the contrast mixture provides contrast between the biofilm, the aqueous-phase and the solid-phase (beads). The imaging method is then applied to two three-dimensional packed-bead columns within which biofilm was grown. Examples of reconstructed images are provided to illustrate the effectiveness of the method. Limitations and applications of the technique are discussed. A key benefit, associated with the presented method, is that it captures a substantial amount of information regarding the topology of the pore-scale transport processes. For example, the quantification of changes in porous media effective parameters, such as dispersion or permeability, induced by biofilm growth, is possible using specific upscaling techniques and numerical analysis. We emphasize that the results presented here serve as a first test of this novel approach; issues with accurate segmentation of the images, optimal concentrations of contrast agents and the potential need for use of synchrotron radiation sources need to be addressed before the method can be used for precise quantitative analysis of biofilm geometry in porous media.

Correspondence to: Yohan Davit, Université de Toulouse; INPT, UPS; IMFT (Institut de Mécanique des Fluides de Toulouse), Allée Camille Soula F-31400 Toulouse, France. Tel: +33-5-3432-2882; fax: +33-5-3432-2993; e-mail: davit@cict.fr

Introduction

Microorganisms (primarily bacteria, fungi and algae), in wet or aqueous environments, tend to aggregate and grow on surfaces, embedded within extracellular polymeric substances (EPS) (Costerton *et al.*, 1995; Sutherland 2001). These sessile communities, termed biofilms, are ubiquitous in industry (Ganesh Kumar & Anand 1998), in medicine and natural environments (Hall-Stoodley *et al.*, 2004). Biofilm cells, when compared with planktonic cells, have been documented to be more resistant to antibiotics and biocides (Costerton *et al.*, 1999; Stewart, 2001; Davies, 2003; Hall-Stoodley *et al.*, 2004). Hence, the development of biofilms can have undesirable and potentially harmful consequences in medical applications (Diosi *et al.*, 2003; Lee & Kim, 2003), but can also be useful in natural or engineered systems such as wastewater treatment processes (Lazarova & Manem, 2000), bioremediation (Rittmann *et al.*, 2000) or CO_2 storage (Mitchell *et al.*, 2009). In medical, natural, as well as engineered systems, biofilm control strategies, based on a better understanding of biofilm growth characteristics as well

as stress response behaviour, have become an important challenge (Stewart *et al.*, 2000; Thormann *et al.*, 2005; Xavier *et al.*, 2005; Rittmann, 2007; Kim *et al.*, 2009).

Within porous media (e.g. subsurface soil or rocks, or the riverine hyporheic zone), biofilm growth within the pore space can induce substantial modifications to mass and momentum transport dynamics (Taylor & Jaffé, 1990; Cunningham *et al.*, 1991; Vandevivere & Baveye, 1992; Wu *et al.*, 1997; Stoodley *et al.*, 2005; Shafahi & Vafai, 2009). Evidence of this type of modification has been developed by observing variation, over time, of macroscopic parameters such as hydraulic conductivity and permeability as well as changes in porosity and dispersion, in conjunction with sampling indicating the presence of biofilm. A large amount of models, based on different conceptual schemes, processes or scales have been developed to describe the growth of biofilm and the associated consequences on porous media transport properties within the last decades. Historically, biofilms have been assumed, for modelling purposes, to form continuous layers (Williamson & McCarty, 1976; Taylor & Jaffé, 1990; Cunningham *et al.*, 1991). Other propositions suggest that biofilms arrange in patchy aggregates within pore throats (Vandevivere & Baveye, 1992). Rittmann (1993) emphasized that both representations can be correct, that is, the spatial distribution of attached microorganisms strongly depends on the physical, chemical and biological properties of the medium and even on its history (Vieira *et al.*, 1993; Telgmann *et al.*, 2004). For example, hydrodynamics, nutrient conditions, microorganism species, predation and bioturbation are found to have a strong impact on the growth dynamics of biofilms. Limitations of these empirical models have been widely discussed, for example interesting analysis concerning the 'microcolony model' (Molz *et al.*, 1986), and the 'biofilm model' (Rittmann & McCarty, 1980) can be found in (Cunningham & Mendoza-Sanchez, 2006) as well as in (Baveye & Valocchi, 1989).

Other models, based on a theoretical and numerical multiscale analysis of the processes, have emerged. For example, cellular automata (Picioreanu *et al.*, 1998; Xavier *et al.*, 2005) have been generally successful and provide interesting perspectives to investigate and understand microorganisms response to various environmental stresses (Molloy, 2006). Individual-based models have also been adapted to the problem of biofilm growth in three- dimensional (3-D) porous structures and can be used to study various phenomena, such as bioclogging (Graf von der Schulenburg *et al.*, 2008). Other mathematical analyses focus on the development of upscaled biofilm-scale and Darcy-scale continuum descriptions of the transport processes. Such methods allow for the establishment of a direct connection between the microscopic topology of the porous medium and the macroscopic continuum behaviour. Various upscaling techniques have been adapted to the problem of biofilms in porous media such as the moment matching method (Dykaar & Kitanidis, 1996) and the volume averaging theory (Wood & Whitaker, 1998; Wood & Whitaker, 1999; Wood *et al.*, 2002; Golfier *et al.*, 2009; Davit *et al.*, 2010). In these theories, effective parameters, for example permeability and dispersion, are numerically calculated on a Representative Elementary Volume.

The fundamental issue with all these models, either empirical or theoretical, continuum or individual based, is that, in the context of porous media, they are often validated only against macroscale experiments, lacking crucial microscale direct observations. Without this microscale information, the multiscale development of pertinent macroscopic models as well as the determination of the fundamental parameters required to characterize the spatio-temporal distribution of biofilm within porous media is difficult. Yet, various methods have been developed for imaging biofilms, including confocal laser scanning microscopy (CLSM) (Lawrence *et al.*, 1991; Kuehn *et al.*, 1998), light microscopy (Bakke & Olsson, 1986; Bakke *et al.*, 2001), electron microscopy (Priester *et al.*, 2007), atomic force microscopy (Beech *et al.*, 1996), nuclear magnetic resonance imaging (Lewandowski *et al.*, 1992; Potter *et al.*, 1996), infrared spectroscopy (Nivens *et al.*, 1993), optical coherence tomography (Xi *et al.*, 2006) and high-frequency ultrasound (Shemesh *et al.*, 2007). Unfortunately, there are constraints associated with each of these imaging techniques. Many of the aforementioned techniques are not applicable to generic porous media structures, due to their inherent opacity. The methods are also not well suited for imaging regions larger than several porous media grains.

To circumvent the opacity problem, most of the work on pore-scale/biofilm-scale observations in porous media has focused on 1-D or 2-D networks (Kuehn *et al.*, 1998; Thullner, 2010a). There has been some discussion of the differences induced by experimental dimensionality (Baveye, 2010; Thullner, 2010a,b). Baveye (2010) suggests that future work should focus on 3-D observations rather than on adapting pseudo 1-D or 2-D results to 3-D configurations. The ability to image biofilm in three dimensions within porous media would considerably aid in providing the experimental data that has been lacking to validate the models that have been presented so far. As a noticeable exception, Seymour *et al.* (2004a,b, 2007) used noninvasive magnetic resonance microscopy to directly observe the 3-D velocity field at the pore-scale and show that biofilm growth can induce anomalous transport. The issue with this technique is that it does not allow spatial resolution of the pore-scale geometry of the different phases within the porous matrix. Recent work presented by (Iltis *et al.*, 2010) focuses on the imaging of biofilm within porous media using monochromatic synchrotron based X-ray computed microtomography. Results from this work illustrate the ability of computed microtomography to provide experimental data for the validation of mathematical models of porous media

associated with biofilm growth. However, the method is based so far on a cumbersome physical straining or on attachment of a contrast agent to the biofilm surface.

In this study, we present a method for imaging non *a priori* labelled microbial biofilms in porous media using a benchtop X-ray computed tomography setup. The presented method allows for the 3-D reconstruction of the solid, aqueous and biofilm phases within a porous matrix with a voxel size of 9 μm. A significant challenge inherent to imaging biofilm within porous media using X-ray absorption tomography lies in selecting proper contrast agents to aid in differentiating between materials with similar absorption coefficients, such as biofilm and water. Most conventional X-ray contrast agents diffuse readily into both the aqueous phase and biofilm (Iltis *et al.*, 2010). The proposed method focuses on the use of a mixture of two different contrast agents that allow for differentiation of the solid, aqueous phase and biofilm regions within the experimental systems evaluated in this study.

The remainder of this paper is organized as follows. First, we present the different protocols that are used in this experimental study. Then, we validate the use of the contrast agents by comparison of 2-D images obtained by (1) optical shadowscopy and (2) X-ray absorption radiography. Finally, the technique is applied to two different model porous media experimental systems containing polyamide or expanded polystyrene beads. Various reconstructed images are shown to illustrate the effectiveness of the method. The limitations of the techniques are discussed as well as suggestions for future work.

Material and methods

The porous models

Three types of porous media models were used for experimentation. Two-dimensional biofilm growth experiments were conducted using a porous media network consisting of expanded polystyrene beads (500–1500 μm) compressed between two PMMA (Plexiglas®), 3-mm-thick, transparent plates. Initial 3-D imaging was conducted using a polystyrene column (3.5 mm inner diameter) packed with 3 mm diameter polyamide beads. Additional 3-D biofilm imaging experiments were conducted using a polystyrene column (3.5 mm ID) packed with polystyrene beads (500–1500 μm). Expanded polystyrene has a lower X-ray absorption coefficient than polyamide, allowing an initial contrast between the biofilm and the beads. Schematics of the experimental devices can be found in Figs 1 and 2 for both the 2-D pore network and the 3-D column experiments.

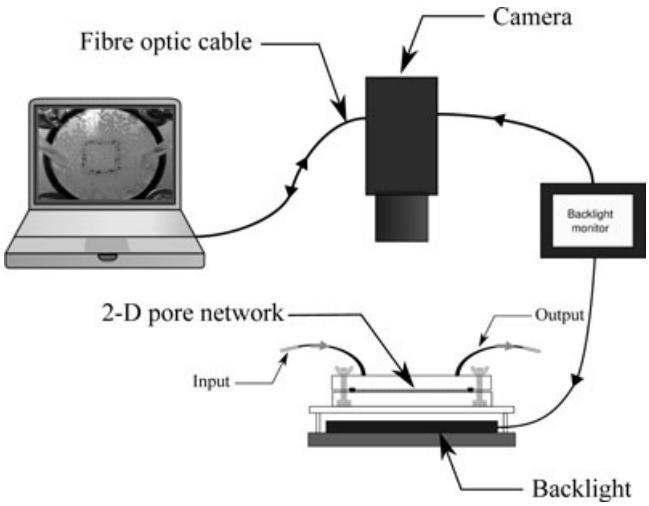

Fig. 2. Optical visualization system for the two-dimensional pore network.

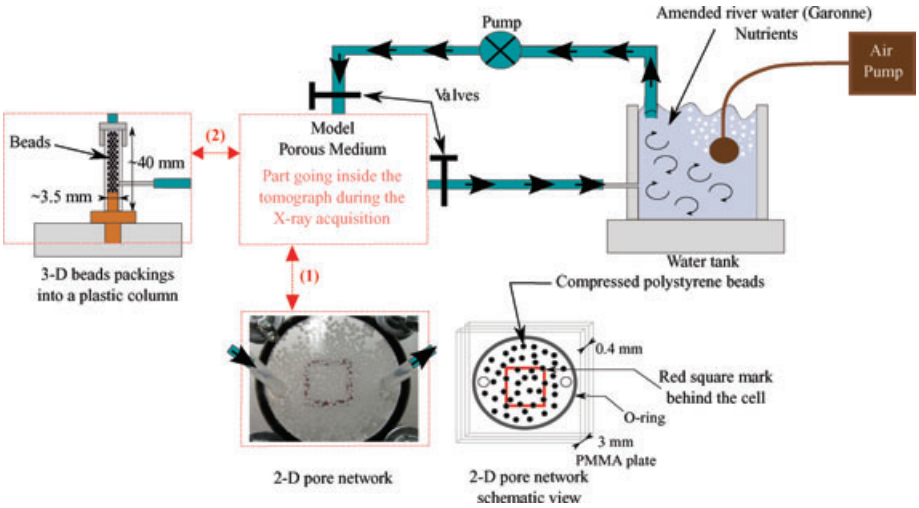

Fig. 1. Flow system used for growing biofilm within (1) the two-dimensional pore network model and (2) the three-dimensional packed bead columns.

Table 1. Biofilm growth experimental design details.

	2-D pore network	3-D polyamide beads	3-D polystyrene beads
Beads diameters	500–1500 μm	3 mm	500–1500 μm
Pump type	Prominent gamma/L diaphragm	Ismatec Mini-S 820 peristaltic	Watson Marlow 505 Du peristaltic
Nutrients			
Introduced at days	0, 3, 6 and 9	0, 4 and 7	0, 3, 6 and 9
$CH_3COONa;\ 3H_2O$	0.66 g	0.16 g	0.66 g
KNO_3	0.33 g	0.06 g	0.33 g
Contrast agents			
C_{BaSO_4}	0.33 g mL^{-1}	0.66 g mL^{-1}	0.33 g mL^{-1}
C_{KI}	0.1 g mL^{-1}	0 g mL^{-1}	0.1 g mL^{-1}
Flow rates	3.5 mL min^{-1}	6 mL min^{-1}	0.07 and 0.5 mL s^{-1}

Growing biofilms

Raw water from the river Garonne (France) was collected, filtered using a 500 μm screen and clarified via sedimentation for approximately 24 h. The river water was further amended with $CH_3COONa;\ 3H_2O$ (carbon source) and KNO_3 (electron acceptor) as indicated in Table 1. The prepared water was then placed in a plastic feed tank used as the reservoir for experimentation and constantly aerated using an air pump. The feed tank was refilled every 24–48 h with prepared river water for the duration of the experiments, to maintain the total water volume between 200 and 400 mL (depending mainly on evaporation). The microbial flora naturally present in the prepared river water was experimentally determined to form sufficient biofilm with the porous media for the purposes of this study. Flow within the experimental systems was induced using either a peristaltic or diaphragm pump (as detailed in Table 1). All experiments were conducted at 20°C ± 1°C in the absence of light to control the growth of phototrophic organisms. Additional details are provided in Table 1.

Contrast agent

As previously mentioned, both the biofilm and the aqueous phase have similar X-ray absorption properties. In addition, all the experimental systems evaluated in this study were designed using plastic materials to minimize the total X-ray exposure time of the microorganisms as well as to optimize the grey-level scaling. Unfortunately, the plastic beads used as the experimental porous medium also have similar X-ray absorption properties to the biofilm and aqueous phase. Hence, obtaining contrast between the different phases requires the utilization of multiple contrast agents. Conventional contrast agents (e.g. potassium iodide) diffuse readily into biofilm when present in the aqueous phase. In this study, we use a medical suspension of micrometre-sized barium sulphate (Micropaque®, Guerbet) to enhance the absorption of the water-phase. Such medical suspensions are conceived to have specific physical properties (Cumberland, 1977; Plouraboué *et al.*, 2004), that is, a high density to provide highly contrasted radiographs, low viscosity to readily penetrate within small sized areas and extremely reduced settling and flocculation of the particles to provide homogeneous absorption of the X-rays. Although barium is usually highly toxic, it is commonly safely used as a medical radiocontrast agent for X-ray imaging of the gastrointestinal tract or angiography because of its insolubility in water. It is also a low-cost product, known not to diffuse within the tissues. The idea behind the utilization of such a suspension is that particles are size excluded from the EPS matrix. If not totally immobilized, micrometre-sized cells within biofilms are known to be greatly constrained in their motion. Hence, diffusion of similar sized barium sulphate particles through the polymeric matrix itself is likely to be negligible. To what extent the contrast agent can penetrate into the biofilm following the flow within nutrients channels and how this depends on the matrix architecture as well as on the contrast agent viscosity and density remains to be fully characterized. It is interesting to emphasize that most studies concerned with convective flows within biofilms involve submicrometre-sized particles (Stoodley *et al.*, 1994) and that micrometre-sized latex beads grown with microbes seem to be immobilized (Drury *et al.*, 1993). In addition, potassium iodide was added to the barium sulphate suspension to provide the required contrast between the polystyrene beads and the biofilm. Various ionic or nonionic iodinated radiocontrast agents are used for medical purposes (Aronson, 2006). In our case, we only require that it readily diffuses within the polymeric matrix. In this context, iodide (whether NaI or KI) has proved to be adapted to X-ray microtomography for noninvasively imaging biological specimens (Chen *et al.*, 2004).

For the polyamide beads, experiments focused on obtaining an important contrast between the biofilm and the water phases, using only barium sulphate at higher concentrations. The details of the contrast agent mixtures used during

experimentation are provided in Table 1. Preliminary scanning of the concentrations ratios were performed; herein, only the concentrations that proved to be the most successful are presented.

Imaging protocols

Two-dimensional imaging. The continuous flow of amended river water through the 2-D flow cells was induced and biofilm was allowed to develop for 10 days at which point optical imaging commenced using the system presented in Fig. 2. A white LED backlight (PHLOX®) applied a uniform illumination of the pore network from beneath the stage and images were captured from above using a 12 bit (SensiCam) camera linked to a computer by a fibre optic cable [as illustrated in Fig. (2)]. Following optical imaging, 10 mL of the contrast agent solution consisting of 0.33 g mL^{-1} barium sulphate and 0.1 g mL^{-1} potassium iodide was injected into the flow cell. The system was then set to rest for approximately 1.5 h to simulate the 3-D X-ray tomography image acquisition time frame (see next section). After this delay, a 2-D X-ray absorption radiograph was captured using a Skyscan 1174 tomograph with a pixel size of 12 μm.

Three-dimensional imaging. After 10 days of continuous flow, the experimental flow cells was removed from the water flow circuit. Ten millilitres of the contrast mixture, containing a suspension of barium sulphate, potassium iodide and water, was slowly injected through the porous model using a syringe. The concentrations of the contrast agent additives for the various experiments evaluated in this study are detailed in Table 1. The experimental flow cells then sat stagnant for approximately 15 min to allow for diffusion of the iodide into the biofilm. During these 15 min, a Skyscan 1174 tomograph was set to a tension voltage of approximately 50 kV and a current of 800 μA. All computed tomography imaging for this study was conducted at a resolution of 9 μm per pixel on a 360° rotation with a rotation step ranging from 0.5° to 0.7°. In each case, the total duration for tomographic imaging is approximately 1.5 h. The major technical limitation we encountered during tomographic imaging was ring artefacts, regardless of the use of the ring artefact reduction option in the commercial software NRecon (SkyScan). Meanwhile, there is no limitation in the method itself which prevents the utilization of synchrotron based tomography (monochromatic) or new generations of scanners capable of producing higher quality images.

Data analysis

Two-dimensional image analysis. 2-D (radiographic) X-ray absorption images (12 bit TIFF images) and 2-D optical images (12 bit TIFF images) were postprocessed using the open source software package ImageJ. For the X-ray images, we applied a fast-Fourier transform bandpass filter to reduce extreme frequency noise. Then, the two data sets are compared using pseudocoloration based on a LookUp Table. This coloration was choosen on the basis of visualization purposes, as guides for the eyes. Quantitative measures, such as correlation ratios, strongly depend on the segmentation procedure. This is beyond the scope of this work to propose such methods; rather, we provide a qualitative analysis of the results. Representative images used for comparison of the two data sets are provided in Fig. 3.

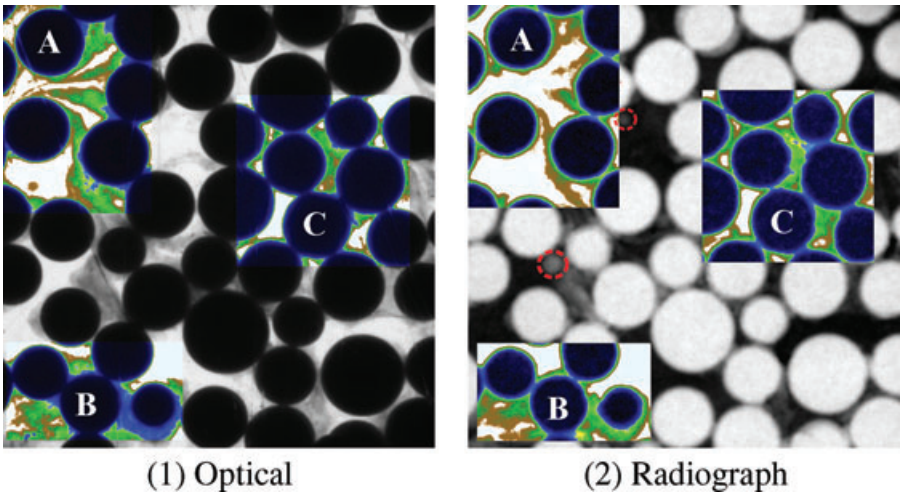

Fig. 3. Comparison of two-dimensional images after 10 days of growth obtained using (1) the visualization device detailed in Figs 2 and (2) Skyscan 1174 X-ray absorption radiograph captured approximately 1.5 h after injection of the contrast agent mixture. On the radiograph, bright corresponds to low X-ray absorption and dark to high X-ray absorption. Three zones A, B and C, assessing various pore-scale geometries, underwent pseudocoloration using ImageJ on the basis of a LookUp Table (LUT). The dark-blue parts correspond to the beads, the blue-green-brown parts to the biofilm and the white parts to the aqueous phase. The parts circled in red on the radiograph correspond to either detached pieces of biofilm or gas bubbles that are not present on the optical shadowscopy.

Three-dimensional tomography. The absorption projection images (12 bit TIFF images) were reconstructed using NRecon to obtain a set of cross-sectional slices (16 bit TIFF images) of the columns, using ring artefact and beam hardening correction. The various greyscale images presented in this paper are encoded as 8 bit images for visualization purposes. For the polyamide beads, images were slightly smoothed and undergo global binarization using ImageJ Otsu's method. The surfaces are built in p3g, surface format, using the commercial software CTAn (Skyscan) and the 3-D geometry is observed using the software CTVol (Skyscan). The goal of this work is to provide an operational technique for imaging biofilm that is to demonstrate that the use of a barium sulphate suspension as a contrast agent is feasible for imaging biofilm within a porous medium matrix.

Results

Two-dimensional experiments

The purpose of the 2-D investigation was to evaluate the behaviour of the contrast agent mixtures and to ensure that sufficient contrast between the various phases was achieved.

Potential issues identified include

Potential issue A. Exclusion of the barium sulphate suspension from the biofilm EPS needs to be verified.

Potential issue B. The contrast agents need to be investigated to see whether interactions between the microorganisms and the contrast agents modify the EPS geometry, thereby preventing the acquisition of representative images.

Potential issue C. The injection of the contrast agent mixture needs to be examined to determine whether the induced shear stress associated with injection results in biofilm detachment from the porous media matrix or in modifications of the EPS geometry.

Potential issue D. It is necessary to determine whether prolonged (1.5 h) X-ray exposure induces changes in the EPS geometry.

The presented X-ray computed tomography imaging method for biofilm investigations is non-invasive, in that the biofilm growth can be imaged *in situ*. However, one caveat that must be taken into account is that X-ray exposure is expected to either severely retard microbial growth or kill the microorganisms all together. Thus, the technique can be considered nondestructive to the porous media–biofilm matrix, but the imaging technique is still terminal.

To investigate possible temporal changes to the biofilm matrix during imaging, a series of experiments were conducted to assess whether the potential issues previously identified as A, B, C and D negatively impact image accuracy and quality on the time-scale of a 3-D tomography acquisition (approximately 1.5 h of exposure time using the Skyscan 1174 tomograph). Thus, images of a 2-D pore network colonized by biofilm obtained using both optical shadowscopy and X-ray computed tomography were compared. Results of the 2-D investigation are presented in Fig. 3. Three zones, corresponding to different biofilm geometries, have been processed using a pseudocoloration to allow for comparison. Within Zone A, three biofilm filaments are clearly visible on both the optical image as well as the X-ray image. In Zones B and C, a clear correlation between the two geometries is apparent although discrepancies between the optical image and X-ray tomography image exist within these zones as well. Based upon the qualitative image comparison within these zones there appears to be good agreement between the two image capturing methods. Because the optical imaging method focuses, primarily, on a top-side view of the biofilm, the increased distribution of barium sulphate within the radiograph can be attributed to an increased flow channel volume within the biofilm that is not visible within the depth of field captured using optical microscopy. Thus the qualitative results presented in Fig. 3 illustrate the utility of using X-rays (and the chosen contrast agent) to image biofilm, particularly when 3-D tomographs are captured as opposed to 2-D radiographs since the tomographs are capable of providing direct visualization of the channelling suspected to be present within the biofilm present in Zones A, B and C. The barium sulphate suspension used for imaging does not appear to enter the EPS layer readily within these zones. Rather the contrast agent seems to follow the aqueous phase flow channels. These conclusions are supported by the results, provided in the next section, concerning the successive use of barium sulphate and iodide. Hence, the issues previously detailed as A and B do not appear to significantly affect our imaging results. However, further investigations are required to elucidate the microscale behaviour of the particles, especially in relation to the density of the EPS matrix and the physical properties of the contrast agent suspension. Nevertheless, the use of barium sulphate as a contrast agent for imaging biofilm within porous media is promising since the delineation of the topology of the flow channels and the associated impact on the transport processes at the pore-scale is definable within relatively large volumes.

With respect to issue C, special care needs to be taken to ensure that the contrast agent or contrast agent mixture is injected at the same flow rate that was applied during the biofilm growth phase or at a lower flow rate to compensate for the slightly larger viscosity of the contrast agents mixture. The introduction of air bubbles during injection should be avoided as well, as this introduces a fourth phase to the imaged system. Although special care was taken during the introduction of the contrast agent mixture used in the collection of the images detailed in Fig. 3, some detachment of biofilm, as well as the introduction of small bubbles into the porous medium, was noted (results are not presented). Within Fig. 3 we have identified, and circled in red, white regions within the radiograph that do not appear within the optical image. In these zones, the X-ray apsorption coefficient is relatively

small, meaning that the concentration of barium sulphate is lower than in the rest of the fluid phase. These are thought to correspond to air bubbles or detached biofilm, in which the contrast agent is volume excluded. However, these effects concern a relatively small proportion of the porous medium and biofilm volume, and this is a problem that can be addressed in future applications by careful experimentation.

Although issue D cannot be fully addressed using this 2-D experiment, we observed no substantial modifications to the EPS geometry after approximately 30 min of X-ray exposure. Although biofilm associated microorganisms are expected to be severely inhibited or killed by exposure to X-rays, the biofilm matrix appears to be stable after exposure times of up to 1.5 h from the benchtop tomography (Skyscan 1174) X-ray source used in this investigation. 3-D results concerning this aspect of the problem are discussed in the next section.

Results of the 3-D tomography and discussion

Single polyamide bead. The first set of 3-D experiments focuses on imaging of biofilm on 3-mm-diameter polyamide beads. For this case, only the barium sulphate suspension was introduced as a contrast agent. Examples of projection data are presented in Fig. 4 at time $t = 0$ without biofilm and at $t = 10$ days following the biofilm growth phase. Differences between these two raw images take the form of patchy white spots meaning, locally, lower X-ray absorption. These zones appear because biofilm has developed, constraining the local volume available for barium sulphate. This set of absorption data is used to reconstruct a set of cross-sectional slices on a single bead within the experimental column. Greyscale images as well as representative binary images are provided in Figs 5(a) and (b) at $t = 0$; Fig. 5(c) and (d) for $t = 10$ days. At $t = 0$, a cross-sectional circular shape, corresponding to the polyamide bead, is observed. After 10 days of biofilm growth, the boundary of the object that we imaged is tortuous and covers more surface. On the basis of the 2-D study presented in the preceding section, we interpret this additional area as biofilm. It is important to note that within Fig. 5(c) there is no contrast between the plastic bead and the biofilm grown on the bead, further reinforcing the proposition that the barium sulphate suspension is excluded from the EPS layer of the biofilm. A solution of potassium iodide was then flushed through the system. A depiction of the polyamide bead after potassium iodide addition is provided as Figs 5(e) and (f). Iodide, when present in the aqueous phase, diffuses readily into biofilm present within the pore space. As a result, the contour of the polyamide bead is all that is clearly visible in Figs 5(e) and (f), thereby confirming that the tortuous zone surrounding the bead in Figs 5(c) and (d) is in fact biofilm. Some bright spots along the edge of the bead on Fig. 5(e) are also visible, corresponding to barium sulphate absorbed on the biofilm.

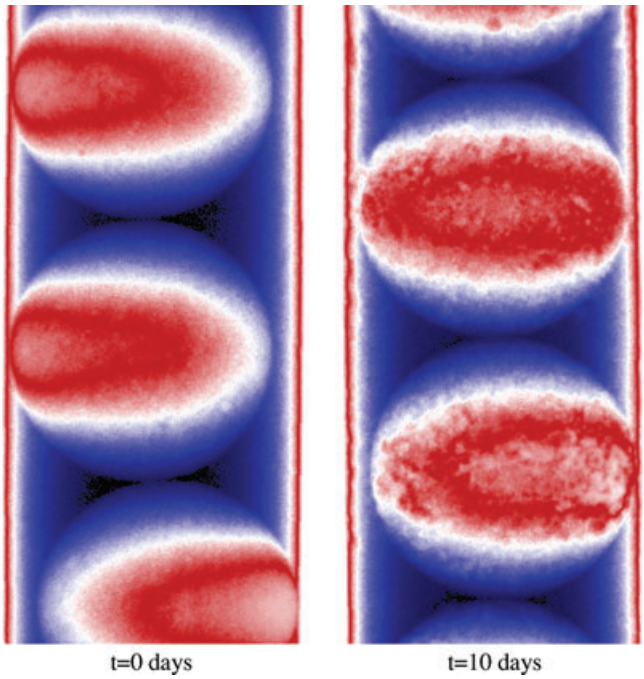

Fig. 4. Examples of projection images obtained with the SkyScan 1174 using BaSO4 as the contrast agent at time $t = 0$ days on the left and $t =$ 10 days on the right. Both images have undertaken a pseudocoloration in ImageJ on the basis of the unionjack LUT (only for visualization purposes). Blue corresponds to the highest X-ray absorption, red to intermediate absorption and white to lowest absorption.

Surface reconstructions of the polyamide bead are provided in Fig. 6. The surface reconstructions correspond to $t = 0$, prior to biofilm growth, and $t = 10$ days, after the biofilm growth phase. Contrast for both images is provided using the barium sulphate suspension. Within the imaged section, the biofilm appears to be highly heterogeneous and represents about 6% of the volume of the naked polyamide bead. Additional study is required to draw further conclusions on biofilm growth and development within our experimental system, however, the ability to image biofilm within porous media using the proposed technique has been established, which is the purpose of this study.

Results for the polydisperse expanded polystyrene beads. For more complex porous structures, such as polydisperse polystyrene beads, the alignment of tomography data captured both prior to, as well as following biofilm growth is not necessarily possible due to the potential for bead displacement due to fluid transport or biofilm growth. Thus, image processing techniques such as image subtraction are not applicable. A mixture of the barium sulphate and potassium iodide contrast agents at two different concentrations was utilized to differentiate between the three materials present within the experimental system. Using this contrast mixture, tomographic imaging was performed. Preliminary imaging was carried out at time $t = 0$ after introducing the contrast agents mixture. Imaging was also conducted at time

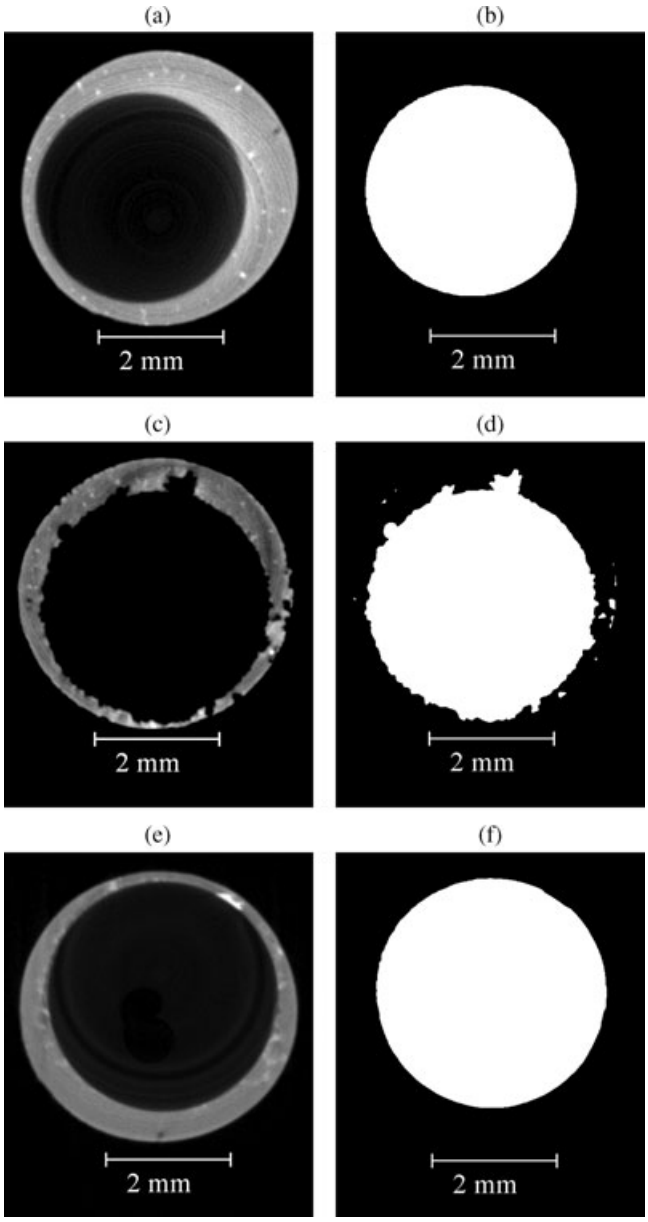

Fig. 5. Cross-sectional reconstructed X-ray computed tomography data for a polyamide bead. Bright corresponds to high X-ray absorption and dark to low X-ray absorption. At $t = 0$ days, with $BaSO_4$ as the contrast agent, (a) is the reconstructed greyscale image and (b) is the binarized image obtained using ImageJ. At $t = 10$ days, after biofilm growth, with $BaSO_4$ as the contrast agent, (c) is the reconstructed greyscale image and (d) is the binarized image obtained using ImageJ. At $t = 10$ days, using potassium iodide as the contrast agent, (e) is the reconstructed greyscale image and (f) is the binarized image obtained using ImageJ. White spots along the edge of the bead on (e) correspond to barium sulphate absorbed on the biofilm.

$t = 10$ days, approximately 15 min after injecting the mixture of both contrast agents. Comparative results are provided in Fig. 7 for the two data sets. Results for the $t = 0$ data set indicate that the contrast agent solution delineates,

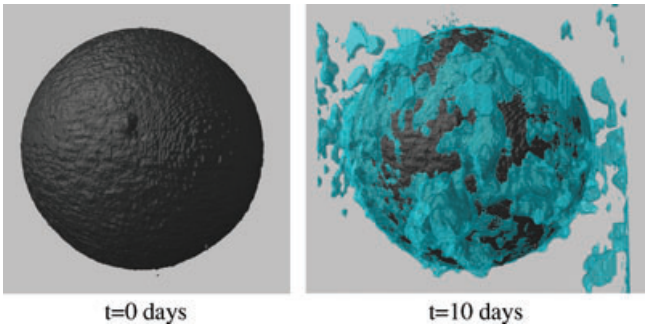

Fig. 6. Three-dimensional surface reconstructions of the polyamide bead at time $t = 0$ using $BaSO_4$ as the contrast agent and the biofilm (soft blue-green) and the polyamide bead (dark) at time $t = 10$ days.

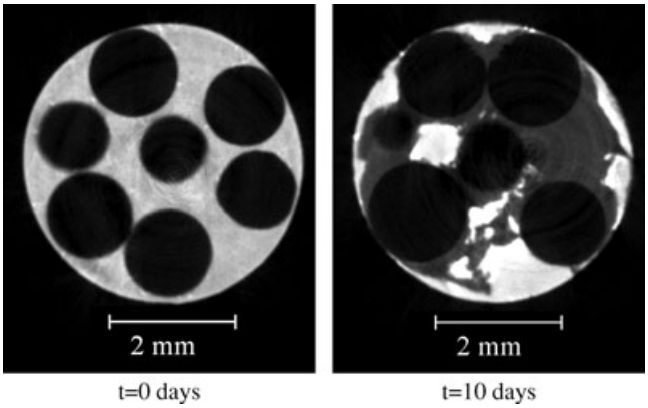

Fig. 7. Greyscale cross-sectional X-ray computed tomography for the experimental columns packed with polystyrene beads at $t = 0$ with the mixture of contrast agents and at time $t = 10$ days. Bright corresponds to high X-ray absorption and dark to low X-ray absorption.

clearly, the beads contained within the column. At $t = 10$ days, the presence of three distinct phases is observed. The brightest phase corresponds to the barium sulphate (highest absorption coefficient). The dark regions correspond to beads and the intermediate greyscale values are interpreted as biofilm which the iodide has diffused into. Figure 8 illustrates the results of a comparative experiment examining biofilm growth within packed bead columns through which two different flow rates were applied. For this experiment, two columns containing polystyrene beads and connected to the same water supply were exposed to flow rates of 0.07 and 0.5 $mL\,s^{-1}$. Within the two columns biofilm growth appears to decrease with increasing flow rate. Although additional experiments are required to draw conclusions about biofilm growth within porous media, the presented results demonstrate that pore-scale information on biofilm growth within a porous medium is readily achievable using the proposed imaging method. Using the results generated using the presented method calculations of column or regional permeability can be performed numerically by solving

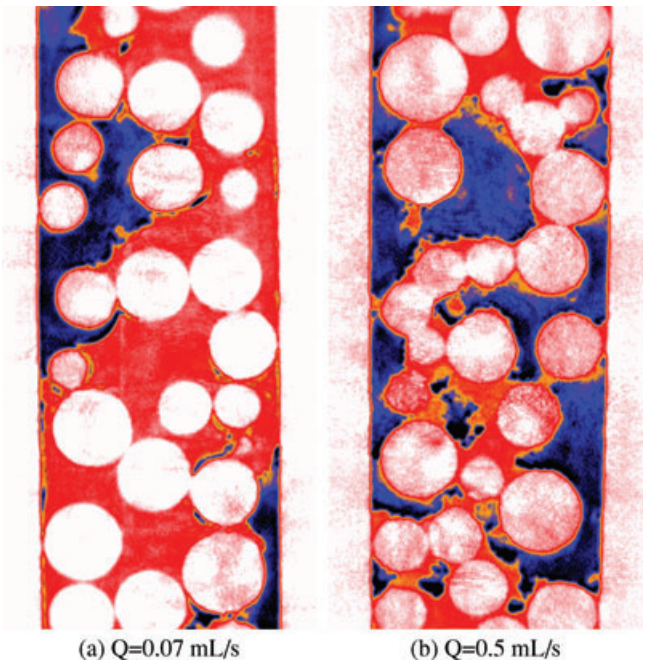

Fig. 8. Examples of reconstructed (X-ray Skyscan 1174 data) sectional slices for the entire length of the column obtained after 10 days at a flow rate of approximately (a) $Q = 0.07$ mL s−1 and (b) $Q = 0.5$ mL s−1 (a pseudocoloration has been applied to the images using ImageJ on the basis of the ceretec LUT and only for visualization purposes). The white-red parts correspond to the beads, the red parts to the biofilm and the blue-dark parts to the aqueous phase.

Navier–Stokes equations. Darcy-scale dispersion tensors can also potentially be calculated using upscaling techniques.

Successive imaging of a single column was conducted in an effort to further evaluate the effect of X-ray exposure on biofilm structure (issue D). The total exposure time was 3 h and consisted of a sequence of two imaging cycles. At the conclusion of this experiment, no change within the biofilm geometry were observable. This suggests that, at least for an acquisition time of 3 h or less, X-rays at the energy emitted by the Skyscan 1174 tomograph (50 kV and 800 μA) do not modify the geometry of the biofilm EPS matrix.

Conclusion

In this study, we present first results for a new method for imaging biofilm in porous media using X-ray computed tomography. We successfully use a mixture of two different contrast agents to obtain a three-phase contrasted 3-D representation of a model porous medium containing solids, water and biofilm. This method, because of its simplicity, accessibility and applicability to complex porous structures, provides an interesting and versatile framework for studying biofilm within porous media systems. The method can potentially be used in the calculation of porous media effective parameters. In particular, the presented method opens possibilities for systematic studies of biofilm response, within porous media, to changes in physical, chemical and biological parameters. For example, modifications of local Reynolds and Péclet numbers, nutrient availability, temperature and pH stresses, and the impact of biofilm biodiversity on biofilm geometry within the 3-D porous media matrix can potentially be investigated. Although the use of synchrotron X-ray sources hold the potential to provide higher quality imaging data and the imaging of biofilm in porous media has been investigated using synchrotron light and silver microspheres as a contrast agent (Iltis *et al.*, 2010), the method presented in this study is functional using both benchtop tomographs, such as the Skyscan 1174 as well as synchrotron X-ray sources, even though more sophisticated image processing procedures need to be developed. Thus the presented method is broadly applicable since imaging is not necessarily restricted by synchrotron accessibility and beam time constraints. On the other hand, one significant limitation associated with the use of benchtop tomographs is that the required imaging time for porous media materials such as glass beads, soil or rock materials is significantly greater than the 1.5 hour image acquisition time reported in this study. As a result, investigations using these types of porous media are anticipated to require synchrotron light sources. Future work will focus on (1) optimization of the image acquisition techniques, to obtain images that can be easily (and impartially) segmented into their respective phases (whether it is using a different polychromatic or a monochromatic imaging system, optimizing the concentrations of the contrast agents, using separate imaging of the solid phase, or similar), (2) a comparison of this work with other 3-D planar imaging techniques such as confocal laser scanning microscopy, for instance to provide further understanding of the interaction between the 1 μm $BaSO_4$ suspension and the architecture of the biofilm, (3) application to real porous samples with heterogeneities of absorption coefficients in the porous structures, and (4) an investigation of microbial retardation or mortality induced by X-ray exposure.

References

Aronson, J. (2006) Iodinated contrast media. *Meyler's Side Effects of Drugs: The International Encyclopedia of Adverse Drug Reactions and Interactions*, 15th edn, pp.1848–1896. Elsevier, Amsterdam.

Bakke, R. & Olsson, P. (1986) Biofilm thickness measurements by light-microscopy. *J. Microbiol. Methods* **5**(22), 93–108.

Bakke, R., Kommedal, R. & Kalvenes, S. (2001) Quantification of biofilm accumulation by an optical approach. *J. Microbiol. Methods* **44**(1), 13–26.

Baveye, P. (2010) Comment on comparison of bioclogging effects in saturated porous media within one- and two-dimensional flow systems by martin thullner. *Ecol. Eng.* **36**(6), 835–836.

Baveye, P. & Valocchi, A. (1989) An evaluation of mathematical models of the transport of biologically reacting solutes in saturated soils and aquifers. *Water Resour. Res.* **25**(6), 1413–1421.

Beech, I., Cheung, C., Johnson, D. & Smith, J. (1996) Comparative studies of bacterial biofilms on steel surfaces using atomic force microscopy and environmental scanning electron microscopy. *Biofouling* **10**(1–3), 65–77.

Chen, V., Li, H. & Fane, A. (2004) Non-invasive observation of synthetic membrane processes—a review of methods. *J. Membr. Sci.* **241**(1), 23–44.

Costerton, J., Lewandowski, Z., Caldwell, D., Korber, D. & Lappin-Scott, H. (1995) Microbial biofilms. *Ann. Rev. Microbiol.* **49**, 711–745.

Costerton, J., Stewart, P. & Greenberg, E. (1999) Bacterial biofilms: a common cause of persistent infections. *Science* **284**(5418), 1318–1322.

Cumberland, D. (1977) Optimum viscosity of barium suspension for use in the double contrast barium meal. *Abdom. Imaging* **2**, 169–174.

Cunningham, A., Characklis, W., Abedeen, F. & Crawford, D. (1991) Influence of biofilm accumulation on porous media hydrodynamics. *Environ. Sci. Technol.* **25**(7), 1305–1311.

Cunningham, J. & Mendoza-Sanchez, I. (2006) Equivalence of two models for biodegradation during contaminant transport in groundwater. *Water Resour. Res.* **42**, W02416.

Davies, D. (2003) Understanding biofilm resistance to antibacterial agents. *Nat. Rev. Drug Discov.* **2**, 881–890.

Davit, Y., Debenest, G., Wood, B.D. & Quintard, M. (2010) Modeling non-equilibrium mass transport in biologically reactive porous media. *Adv. Water Resour.*, doi:10.1016/j.advwatres.2010.06.013.

Diosi, G., Telegdi, J., Farkas, G., Gazso, L. & Bokori, E. (2003) Corrosion influenced by biofilms during wet nuclear waste storage. *Int. Biodeterior. Biodegradation* **51**(2), 151–156.

Drury, W., Characklis, W. & Stewart, P. (1993) Interactions of 1 μm latex particles with pseudomonas aeruginosa biofilms. *Water Res.* **27**(7), 1119–1126.

Dykaar, B. & Kitanidis, P. (1996) Macrotransport of a biologically reacting solute through porous media. *Water Resour. Res.* **32**(2), 307–320. Available at http://www.agu.org/pubs/crossref/1996/95WR03241.shtml

Ganesh Kumar, C. & Anand, S. (1998) Significance of microbial biofilms in food industry: a review. *Int. J. Food Microbiol.* **42**(1–2), 9–27.

Golfier, F., Wood, B., Orgogozo, L., Quintard, M. & Buès, M. (2009) Biofilms in porous media: development of macroscopic transport equations via volume averaging with closure for local mass equilibrium conditions. *Adv. Water Resour.* **32**(3), 463–485.

Graf von der Schulenburg, D., Pintelon, T., Picioreanu, C., Van Loosdrecht, M. & Johns,M. (2008) Three-dimensional simulations of biofilm growth in porous media. *AIChE J.* **55**(2), 494–504.

Hall-Stoodley, L., Costerton, J. & Stoodley, P. (2004) Bacterial biofilms: from the natural environment to infectious diseases. *Nat. Rev. Microbiol.* **2**, 95–108.

Iltis, G., Armstrong, R., Jansik, D., Wood, B. & Wildenschild, D. (2010) Imaging biofilm architecture within porous media using synchrotron based x-ray computed microtomography. *Water Resour. Res.*, submitted.

Kim, J., Choi, H. & Pachepsky, Y. (2009) Biofilm morphology as related to the porous media clogging. *Water Res.,* **44**(4), 1193–1201.

Kuehn, M., Hausner, M., Bungartz, H., Wagner, M., Wilderer, P. & Wuertz, S. (1998) Automated confocal laser scanning microscopy and semiautomated image processing for analysis of biofilms. *Appl. Environ. Microbiol.* **64**, 4115–4127.

Lawrence, J., Hoyle, D.K., Costerton, J. & Caldwell, D. (1991) Optical sectioning of microbial biofilms. *J. Bacteriol.* **173**, 6558–6567.

Lazarova, V. & Manem, J. (2000) Innovative biofilm treatment technologies for water and wastewater treatment. Biofilms II. Process Analysis and Applications. Wiley-Liss, New York, pp. 159–206.

Lee, D. & Kim, S. (2003) Bacterial species in biofilm cultivated from the end of the seoul water dirstribution system. *J. Appl. Microbiol.* **95**(2), 317–324.

Lewandowski, Z., Altobelli, S., Majors, P. & Fukushima, E. (1992) NMR imaging of hydrodynamics near microbially colonized surfaces. *Water Sci. Technol.* **26**, 577–584.

Mermillod-Blondin, F., Gaudet, J., Gerino, M., Desrosiers, G., José, J. & Creuzé des Châtelliers, M. (2004) Relative influence of bioturbation and predation on organic matter processing in river sediments: a microcosm experiment. *Freshwater Biol.* **49**(7), 895–912.

Mitchell, A., Phillips, A., Hiebert, R., Gerlach, R., Spangler, L. & Cunningham, A. (2009) Biofilm enhanced geologic sequestration of supercritical CO_2. *Int. J. Greenhouse Gas Control* **3**(1), 90–99.

Molloy, S. (2006) Biofilms: you do the maths *Nat. Rev. Microbiol.* 4, 4.

Molz, F., Widdowson, M. & Benefield, L. (1986) Simulation of microbial growth dynamics coupled to nutrient and oxygen transport in porous media. *Water Resour. Res.* **22**, 1207–1216.

Nivens, D., Chambers, J., Anderson, T., Tunlid, A., Smit, J. & White, D. (1993) Monitoring microbial adhesion and biofilm formation by attenuated total reflection fourier-transform infrared-spectroscopy. *J. Microbiol. Methods* **17**(3), 199–213.

Picioreanu, C., van Loosdrecht, M. & Heijnen, J. (1998) Mathematical modeling of biofilm structure with a hybrid differential-discrete cellular automaton approach. *Biotechnol. Bioeng.* **58**(1), 101–116.

Plouraboué, F., Cloetens, P., Fonta, C., Steyer, A., Lauwers, F. & Marc-Vergnes, J. (2004) X-ray high-resolution vascular network imaging. *J. Microsc.* **215**, 139–148.

Potter, K., Kleinberg, R., McFarland, E. & Brockman, F. (1996) Assay for bacteria in porous media by diffusion-weighted NMR. *J. Magn. Reson. B* **113**(1), 9–15.

Priester, J., Horst, A., Van De Werfhorst, L., Saleta, J., Mertes, L. & Holden, P. (2007) Enhanced visualization of microbial biofilms by staining and environmental scanning electron microscopy. *J. Microbiol. Methods* **68**(3), 577–587.

Rittmann, B. (1993) The significance of biofilms in porous media. *Water Resour. Res.* **29**(7), 2195–2202.

Rittmann, B. (2007) Where are we with biofilms now? where are we going?. *Water Sci. Technol.* **55**(8–9), 1–7.

Rittmann, B. & McCarty, P. (1980) Model of steady-state-biofilm kinetics. *Biotechnol. Bioeng.* **22**(11), 2343–2357.

Rittmann, B., Schwarz, A. & Saez, P. (2000) Biofilms applied to hazardous waste treatment. Biofilms II. Process Analysis and Applications. Wiley-Liss, New York, pp. 159–206.

Seymour, J., Codd, S., Gjersing, E. & Stewart, P. (2004a) Magnetic resonance microscopy of biofilm structure and impact on transport in a capillary bioreactor. *J. Magn. Reson.* **167**(2), 322–327.

Seymour, J., Gage, J., Codd,S. & Guerlach, R. (2004b) Anomalous fluid transport in porous media induced by biofilm growth. *Phys. Rev. Lett.* **93**(19), 198103.1–198103.4.

Seymour, J., Gage, J., Codd, S. & Guerlach, R. (2007) Magnetic resonance microscopy of biofouling induced scale dependent transport in porous media. *Adv. Water Resour.* **30**(6–7), 1408–1420.

Shafahi, M. & Vafai, K. (2009) Biofilm affected characteristics of porous structures. *Int. J. Heat Mass Transfer* **52**(3–4), 574–581.

Shemesh, H., Goertz, D., van der Sluis, L., de Jong, N., Wu, M. & Wesselink, P. (2007) High frequency ultrasound imaging of a single-species biofilm. *J. Dentistry* **35**(8), 673–678.

Stewart, P. (2001) Multicellular resistance: Biofilms. *Trends Microbiol.* **9**(5), 204.

Stewart, P., McFeters, G. & Huang, C. (2000) Biofilm Control by Antimicrobial Agents. Wiley-Liss, New York, pp. 159–206.

Stoodley, P., deBeer, D. & Lewandowski, Z. (1994) Liquid flow in biofilm systems. *Appl. Environ. Microbiol.* **60**, 2711–2716.

Stoodley, P., Dodds, I., De Beer, D., Scott, H. & Boyle, J. (2005) Flowing biofilms as a transport mechanism for biomass through porous media under laminar and turbulent conditions in a laboratory reactor system. *Biofouling* **21**(3–4), 161–168.

Sutherland, I. (2001) Biofilm exopolysaccharides: a strong and sticky framework. *Microbiology* **147**, 3–9.

Taylor, S. & Jaffé, P. (1990) Biofilm growth and the related changes in the physical properties of a porous medium, 1, experimental investigation. *Water Resour. Res.* **26**(9), 2153–2159.

Telgmann, U., Horn, H. & Morgenroth, E. (2004) Influence of growth history on sloughing and erosion from biofilms. *Water Res.* **38**(17), 3671–3684.

Thormann, K., Saville, R., Shukla, S. & Spormann, A. (2005) Induction of rapid detachment in *Shewanella oneidensis* mr-1 biofilms. *J. Bacteriol.* **187**(3), 1014–1021.

Thullner, M. (2010a). Comparison of bioclogging effects in saturated porous media within one- and two-dimensional flow systems. *Ecol. Eng.* **36**(2), 176–196.

Thullner, M. (2010b). Response to comment on comparison of bioclogging effects in saturated porous media within one- and two-dimensional flow systems by Martin Thullner by Philippe Baveye. *Ecol. Eng.*, **36**(6), 837–838.

Vandevivere, P. & Baveye, P. (1992) Saturated hydraulic conductivity reduction caused by aerobic bacteria in sand columns. *Soil Sci. Soc. Am. J.* **156**, 1–13.

Vieira, M., Melo, L. & Pinheiro, M. (1993) Biofilm formation: hydrodynamic effects on internal diffusion and structure. *Biofouling* **7**(1), 67–80.

Williamson, K. & McCarty, P. (1976) A model of substrate utilization by bacterial films. *J. Water Pollut. Control Fed.* **48**(1), 9–24.

Wood, B., Quintard, M. & Whitaker, S. (2002) Calculation of effective diffusivities for biofilms and tissues. *Biotechnol. Bioeng.* **77**(5), 495–516. Available at URLhttp://dx.doi.org/10.1002/bit.10075

Wood, B. & Whitaker, S. (1998). Diffusion and reaction in biofilms. *Chem. Eng. Sci.* **53**(3), 397–425.

Wood, B. & Whitaker, S. (1999) Cellular growth in biofilms. *Biotechnol. Bioeng.* **64**(6), 656–670.

Wu, J., Gui, S., Stahl, P. & Zhang, R. (1997) Experimental study on the reduction of soil hydraulic conductivity by enhanced biomass growth. *Soil Sci.* **162**(10), 741–748.

Xavier, J., Picioreanu, C., Rani, S., van Loosdrecht, M. & Stewart, P. (2005) Biofilm-control strategies based on enzymic disruption of the extracellular polymeric substance matrix—a modelling study. *Microbiology* **151**, 3817–3832.

Xi, C., Marks, D., Schlachter, S., Luo, W. & Boppart, S. (2006) High-resolution three-dimensional imaging of biofilm development using optical coherence tomography. *J. Biomed. Opt.* **11**(3), 034001.